Strange attractors in weakly turbulent Couette-Taylor flow

A. Brandstater and Harry L. Swinney
Department of Physics and the Center for Nonlinear Dynamics, The University of Texas, Austin, Texas 78712-9990
(Received 7 August 1986)

We have conducted an experiment on the transition from quasiperiodic to weakly turbulent flow of a fluid contained between concentric cylinders with the inner cylinder rotating and the outer cylinder at rest. Power spectra, phase-space portraits, and circle maps obtained from velocity time-series data indicate that the nonperiodic behavior which we have observed is deterministic, that is, it is described by strange attractors. We discuss various problems that arise in computing the dimension of strange attractors constructed from experimental data and show that these problems impose severe requirements on the quantity and accuracy of data necessary for determining dimensions greater than about 5. In the present experiment the attractor dimension increases from 2 at the onset of turbulence to about 4 at a Reynolds number 50% above the onset of turbulence.

I. INTRODUCTION

The determination of the fractal dimension d of strange attractors has become a standard diagnostic tool in the analysis of dynamical systems.[1–5] The dimension, roughly speaking, measures the number of degrees of freedom that are relevant to the dynamics. Most work on dimension has concerned maps, such as the Hénon map, or systems given by a few coupled ordinary differential equations, such as the Lorenz and Rössler models. For any chaotic system described by differential equations, d must be greater than 2, but d could be much much larger for a system described by *partial* differential equations, such as the Navier-Stokes equations. Indeed, the best rigorous estimates of the dimension of attractors for turbulent flow yield quite large numbers for the attractor dimension (say 10^8).[6–8]

Recent experiments on the transition to chaos in the Couette-Taylor system,[9] convection,[10] and a differentially heated annulus[11] have shown that the chaotic (strange) attractors for these systems have surprisingly low dimension. However, efforts to compute dimension from experimental data have revealed a number of problems that do not arise in the analysis of model systems where essentially unlimited amounts of data of arbitrary accuracy can easily be generated.[3,5] Using our Couette-Taylor data as an example, we will examine in this paper some of the problems that arise in determining dimension from laboratory data.

After a brief discussion of the experimental methods in Sec. II, we will show in Sec. III that photographs, velocity power spectra, phase-space portraits, and circle maps alone provide evidence that the observed nonperiodic behavior is *deterministic* and *low dimensional*, that is, *chaotic*. In Sec. IV we present the dimension calculations, emphasizing the limitations and possible pitfalls in such calculations. Section V is a discussion and summary.

II. EXPERIMENTAL METHODS

The Reynolds number for the Couette-Taylor system can be defined as $R = a\Omega(b-a)/\nu$, where a and b are, respectively, the radii of the inner and outer cylinders, Ω is the angular velocity of the inner cylinder, and ν is the kinematic viscosity. In our system we have $a = 5.205$ cm and $b = 5.947$ cm, which gives a radius ratio of 0.875. At this radius ratio the critical Reynolds number for the onset of Taylor vortex flow in an infinite system is $R_c = 118.4$.[12] The upper and lower boundaries of the annulus are Teflon rings that are fastened to the outer cylinder, and the ratio of the fluid height to the gap between the cylinders is 20.0. The frequency of rotation of the inner cylinder is locked to a crystal reference oscillator.

The working fluid is orange oil (Cargille No. 19604), chosen because it has the same index of refraction at the laser wavelength (488 nm) as the borosilicate glass outer cylinder. The fluid kinematic viscosity is 0.0109 cm^2/s at 25 °C. In the laser Doppler velocimetry measurements the fluid is seeded with 0.22-μm diam spherical titanium dioxide particles, and the flow visualization studies are made using a dilute suspension of small platelet particles (Kalliroscope AQ1000, Ref. 13). The cylinder system is immersed in a bath that is controlled in temperature to 0.1 °C. The bath has the same refractive index as the glass cylinder and the working fluid, and the windows of the bath are parallel glass plates; therefore, the optics are all planar for the laser Doppler velocimetry measurements.

The radial component of the velocity is measured (at points midway in the gap between the inner and outer cylinders) by the laser Doppler crossed-beam technique. A 256-channel pulse correlator is used to determine the correlation function of the pulse train from the photomultiplier; each pulse corresponds to the detection of a single photon. In the Reynolds-number range of interest the signal is sufficiently strong so that a correlation function (oscillating at the Doppler shift frequency) can be obtained in a time that is short compared to the time required for the velocity to change significantly—if needed, as many as 100 velocity points can be obtained per characteristic oscillation period. Thus the Doppler shifts extracted from the correlation functions at successive time intervals yield essentially the instantaneous velocity.[14,15] The velo-

city data files each contain 32 768 points.

The spatial resolution of the laser Doppler measurements is set by the size of the scattering volume. This sample volume is approximately an ellipsoid of revolution of length 100 μm in the azimuthal direction and 30 μm in the axial and radial directions; for comparison, the gap between the cylinders is 7.42 mm. The concentration of the 0.22-μm diam spherical seed particles is adjusted so that the scattering volume contains about one particle on the average.

III. DETERMINISTIC NONPERIODIC FLOW (CHAOS)

A. Photographs, time series, and spectra

Previous experiments have shown that the Couette-Taylor system with a radius ratio of 0.875 and aspect ratio around 20 passes through the following sequence of well-defined states as the Reynolds number is increased:[16–18] the basic (Couette) flow; Taylor vortex flow, which is time independent; wavy vortex flow, which is periodic in time; modulated wavy vortex flow, which is quasiperiodic; and, finally, chaotic (weakly turbulent) flow. In this paper we are concerned with the transition from modulated wavy vortex flow to chaos. Figure 1 shows photographs of the flow for a sequence of Reynolds numbers ranging from $R/R_c=10.6$, which is in the modulated wavy vortex flow regime, to $R/R_c=26.3$, which is well beyond the onset of chaos ($R/R_c=11.7\pm0.2$).[19]

The photographs show that some small-scale spatial structure is discernible below the onset of chaos, but the small-scale structure in successive vortex pairs appears to be the same. Above the onset of chaos there is an increasing amount of small-scale structure, and it is no longer the same in different vortex pairs. Nevertheless, a high degree of spatial order persists above the onset of chaos; therefore, we prefer to call this flow chaotic rather than turbulent, but, following current usage, we also sometimes call this flow "weakly turbulent." The increase in the number of degrees of freedom with increasing Reynolds number, qualitatively clear from the photographs, will be quantified by the dimension calculations given in Sec. IV.

Velocity time series and power spectra are shown for a sequence of Reynolds numbers in Figs. 2 and 3, respectively. In Figs. 2, 3(a), and 3(b) the upper two graphs are for modulated wavy vortex flow, while the lower two graphs in each figure are for chaotic flow. In modulated wavy vortex flow there are two traveling azimuthal waves[17,18] on the Taylor vortices, the first with rotation frequency $\omega_1/m_1\Omega=0.34$ and the second with rotation frequency $\omega_2/m_2\Omega=0.44$; in the present experiment the azimuthal wave numbers for both waves were the same, $m_1=m_2=4$. The values 0.34 and 0.44 for the wave frequencies are approximate; actually the ratio ω_2/ω_1 increases slowly but in a strictly monotone fashion with increasing Reynolds number in the vicinity of the onset of chaos—*no* frequency locking is observed.[20]

The velocity power spectra for modulated wavy vortex flow contain two fundamental frequency components and their combinations, as Fig. 3 illustrates with data at $R/R_c=10.4$ and 11.4. The background level in these two spectra is instrumental noise rather than fluid noise; the instrumental noise is white and independent of Reynolds number [see Fig. 3(b)]. The onset of nonperiodic flow is marked by a rise in the background noise above the instrumental noise level, as can be seen in the spectra at $R/R_c=12.0$ and 15.5. However, even at $R/R_c=15.5$ most of the spectral energy is still in the components at ω_1 and ω_2 (and their combinations), and the flow is still highly ordered, as can be seen in the photographs in Fig. 1. At larger Reynolds numbers the amplitudes of the components at ω_1 and ω_2 decrease with increasing Reynolds number, and these components disappear at $R/R_c=22.0$ and 20.0, respectively.[9,16,21]

B. Spectral evidence for deterministic behavior

Broadband noise in power spectra can arise from stochastic or deterministic processes, but the decay in the spectral power at large ω is different for the two cases.[22,23] For a process governed by an nth-order *stochastic* differential equation, Sigeti and Horsthemke[23] have shown that the spectral power at high frequencies follows a power law, $P(\omega)\propto\omega^{-2n}$. In contrast, the assumption that the solution of *deterministic* equations is infinitely differentiable leads to the conclusion that the spectrum falls off exponentially, or at least faster than ω^{-s} for arbitrarily large s. Greenside *et al.*[22] examined numerically a stochastic differential equation model and a deterministic model, and they found a power-law decay for the first case (with n equal to the order of the equation, 2) and an exponential decay for the second case, which was the Lorenz model.

Greenside *et al.* analyzed data obtained by Ahlers and co-workers[24] for weakly turbulent convection and found power-law behaviors, ω^{-4} in some cases and ω^{-2} in other cases. Another study of turbulent convection, by Atten *et al.*,[25] showed exponential decay at high frequencies.

Figure 4 shows two graphs of our velocity power spectra obtained at $R/R_c=15.2$, one on a semilogarithmic scale and the other on a log-log scale. The exponential decay given by the linear behavior on the semilogarithmic plot indicates that the noise in our data arises from a deterministic rather than a stochastic process.

C. Phase space portraits and Poincaré sections

We have constructed multidimensional phase-space portraits from the velocity time series $\{V(t_k);\ t_k=k\,\Delta t,\ k=1,\ldots,32\,768\}$ by the method of time delays:[26,27] trajectories in an m-dimensional space pass through the points $\{V(t_k),\ V(t_k+\tau),\ldots,V(t_k+(m-1)\tau)\}$, where m is the embedding dimension and τ is a time delay.

For an infinite amount of noise-free data the choice of time delay τ is arbitrary,[27] but for real laboratory data a good choice of τ is essential for geometrical as well as numerical analysis of a phase portrait. As $\tau\to0$, the trajectory approaches the identity line $V(t)=V(t+p\tau)$ for all positive integers $p<m$. There are other values of τ for which the data points are concentrated in a small region of phase space, so that the local structure of the attractor

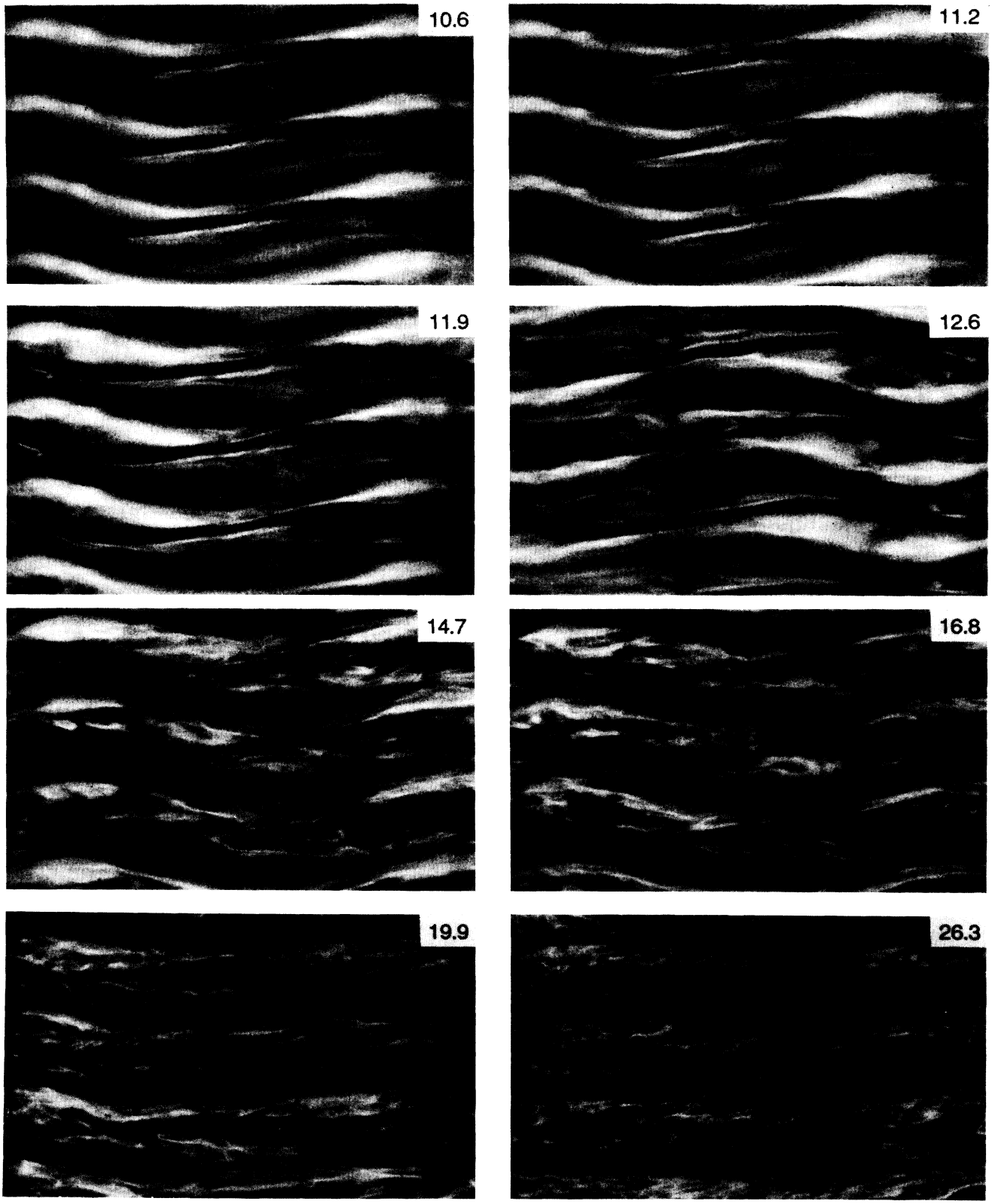

FIG. 1. Photographs of the flow as a function of Reynolds number in the region of transition from modulated wavy vortex flow to chaotic flow. The values of R/R_c are given on the photographs. The first two pictures are of modulated wavy vortex flow, while the remainder are in the chaotic regime. The flow patterns were rendered visible using a suspension of small platelets (Ref. 13).

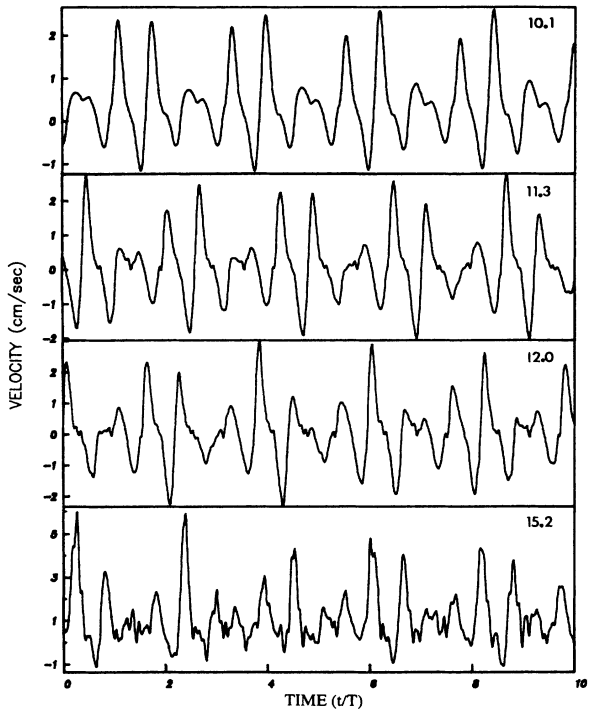

FIG. 2. The time dependence of the radial component of the velocity, measured at a point in the middle of the gap between the inner and outer cylinders, for two Reynolds numbers ($R/R_c = 10.1$ and 11.3) corresponding to modulated wavy vortex flow, and two Reynolds numbers ($R/R_c = 12.0$ and 15.2) corresponding to chaotic flow. The corresponding power spectra are shown in Fig. 3. The time T is the period of rotation of the inner cylinder; in seconds, $T = 18.76/(R/R_c)$.

cannot be extracted from the reconstructed phase portraits.

Recently Fraser and Swinney[28,29] have shown that the optimum choice of τ in most systems corresponds to the first local minimum in the mutual information function,

$$I = \int \int P(X,Y)\log_2[P(X,Y)/P(X)P(Y)]dX\,dY\ ,$$

where, in the present case, $X = V(t)$ and $Y = V(t+\tau)$, so $I = I(\tau)$. $P(X)$ and $P(X,Y)$ are, respectively, the probability density and the joint probability density. The mutual information measures the dependence of two variables in a more general way than the autocorrelation function, which measures the *linear* dependence. The mutual information gives the accuracy in the prediction of the value of $V(t+\tau)$, given the value of $V(t)$. Now if $V(t)$ and $V(t+\tau)$ are to be used as coordinates in constructing a phase portrait, these coordinates should be as independent as possible. Therefore, the optimum choice in τ corresponds to a minimum in the mutual information function. The first minimum is preferable over later minima because as time passes the points on the attractor spread out over the invariant measure.

Figure 5 shows the mutual information as a function of τ for the Couette-Taylor flow data obtained at

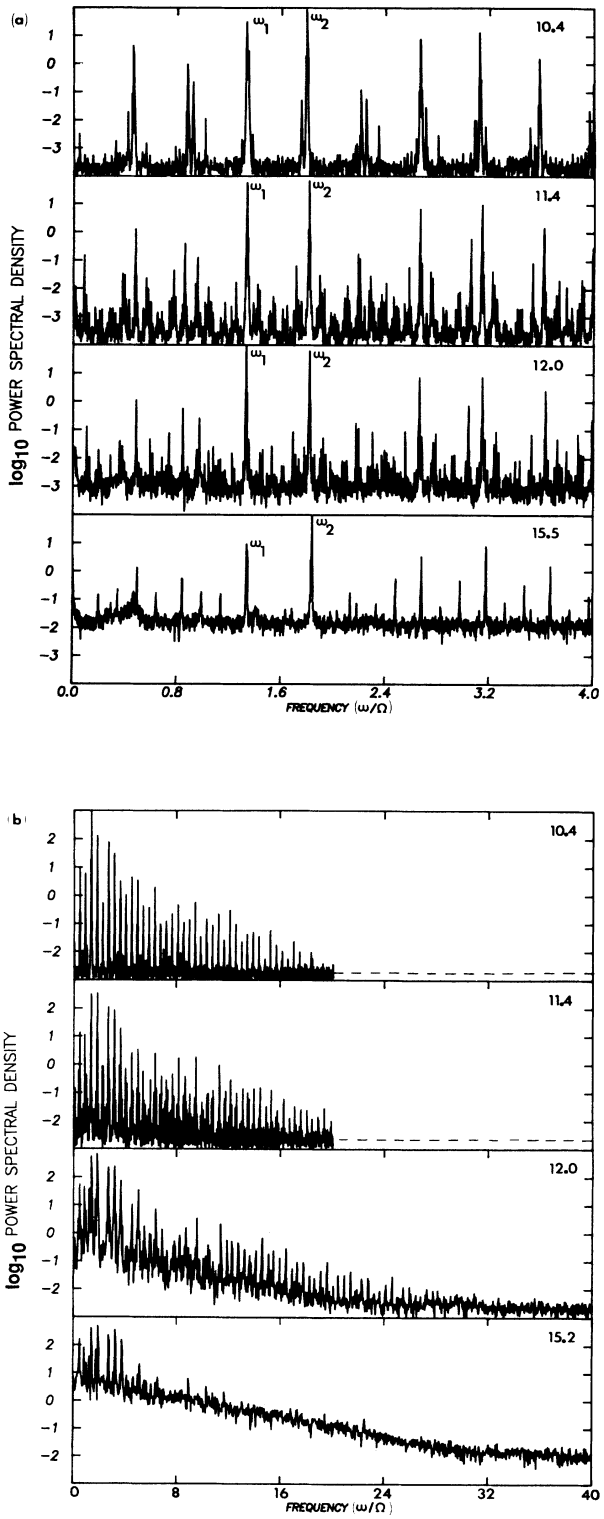

FIG. 3. Velocity power spectra showing (a) low-frequency and (b) high-frequency behavior for quasiperiodic modulated wavy vortex flow at $R/R_c = 10.4$ and 11.4 and chaotic flow at $R/R_c = 12.0$ and 15.5. The frequency scales are in units of the cylinder frequency Ω.

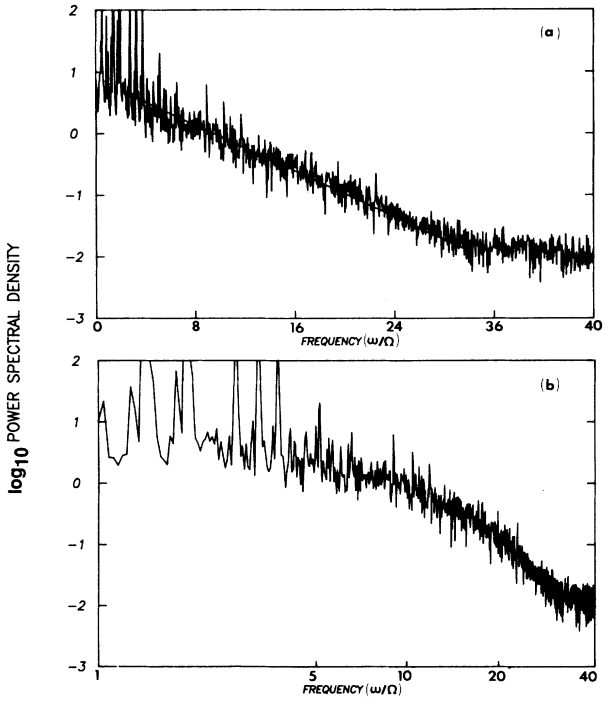

FIG. 4. (a) A semilogarithmic velocity power spectrum and (b) a log-log spectrum for data obtained at $R/R_c = 15.5$. The exponential decay (straight-line behavior) down to the instrumental noise level (10^{-2}) is clear in (a).

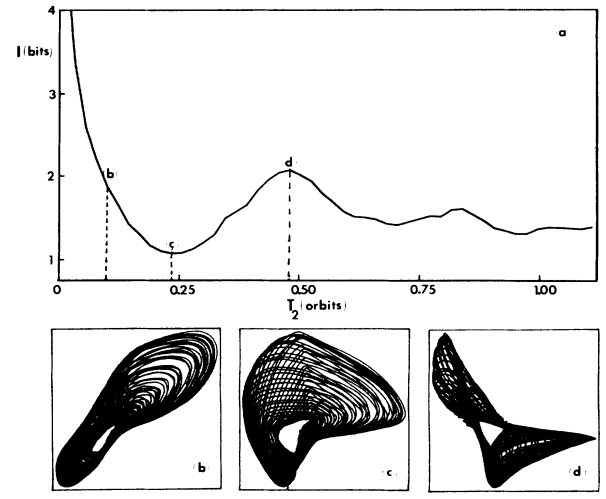

FIG. 5. (a) The mutual information is plotted as a function of time delay τ for data obtained at $R/R_c = 10.1$. The time delay is given relative to the period T_2 of the second fundamental frequency ω_2. Two-dimensional projections of phase portraits, $V(t+\tau)$ versus $V(t)$, constructed for three different time delays, are shown below the graph of the mutual information: (b) $\tau/T_2 = 0.11$, which is too small a delay time; (c) $\tau/T_2 = 0.24$, corresponding to the first minimum in the mutual information, this is the optimum choice for τ; (d) $\tau/T_2 = 0.48$, which is too large a delay time.

$R/R_c = 10.1$. For these data and for all other data presented in this paper the first minimum in the mutual information occurs for a delay time about equal to one-fourth of the period of the second fundamental frequency, ω_2. Delay times near this optimum value were used in our analysis.

Figure 6(a) shows phase portraits obtained for a sequence of Reynolds numbers, and Fig. 6(b) shows the corresponding Poincaré sections given by the intersection of orbits in three-dimensional phase portraits with planes. At $R/R_c = 10.1$ and 11.3 the Poincaré sections clearly show that the orbits lie on the surface of a torus; the scatter presumably arises from instrumental noise. Even at $R/R_c = 12.0$, where the photographs, time series, and power spectra indicate the presence of noise, the torus is still evident, although it is much noisier and it has developed prominent wrinkles. With our data files of about 300 orbits we were unable to quantify the folding at the wrinkles.

D. Lyapunov exponents

Lyapunov exponents characterize the exponentially fast divergence or convergence of nearby trajectories in phase space. The largest Lyapunov exponent is zero for a limit cycle, a 2-torus, or, more generally, an n-torus, but at the onset of chaos the largest Lyapunov exponent becomes positive. Wolf *et al.*[30] have developed a method for computing Lyapunov exponents from experimental data, and that method has been applied to our data for the Couette-Taylor system.[9] The conclusion was that the largest Lyapunov exponent becomes positive at $R/R_c = 11.7 \pm 0.2$, which is in accord with the other evidence for the onset of chaos.

E. Circle maps and the onset of chaos

One-dimensional maps of circle, θ_{n+1} versus θ_n, can be constructed from the Poincaré sections of a 2-torus, as shown in Fig. 7: θ_n is the angle of the nth point measured with respect to a polar coordinate system whose origin is inside the closed loop formed by the Poincaré section. Figure 7 shows that this construction yields smooth curves for the function $\theta_{n+1} = f(\theta_n)$, even beyond the onset of chaos. This is further evidence that the nonperiodic flow is deterministic—given θ_n, the map *determines* θ_{n+1}.

Extensive recent studies of circle maps have been motivated by the interest in characterizing the transition from quasiperiodic flow on a 2-torus to chaos.[31–35] Circle maps with cubic inflection points have been found to exhibit *universal* behavior in the vicinity of the control parameter value at which the map becomes noninvertible. As the point of noninvertibility of the map is approached, there is an increasing probability that the winding number of the map, which corresponds to the ratio of the two frequencies of the quasiperiodic flow, will become locked at a rational number value. The theory predicts the scaling behavior of these frequency-locked bands. At the critical point, where the map becomes noninvertible, only frequency-locked states occur. Thus frequency locking plays a crucial role in the large body of theory that has

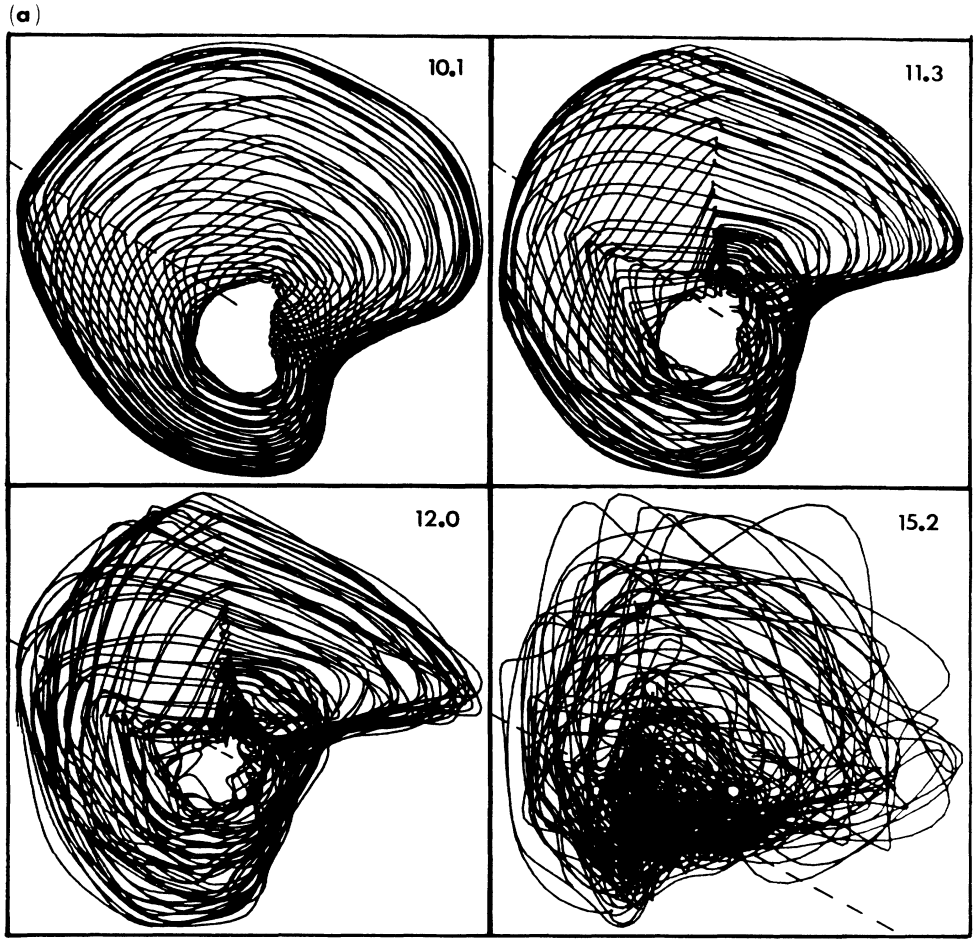

FIG. 6. (a) Two-dimensional phase portraits $V(t+\tau)$ versus $V(t)$ constructed for two Reynolds numbers ($R/R_c = 10.1$ and 11.3) corresponding to modulated wavy vortex flow and two Reynolds numbers ($R/R_c = 12.0$ and 15.2) corresponding to chaotic flow. (b) Poincaré sections given by the intersection of orbits of three-dimensional phase portraits [where the third axis is $V(t+2\tau)$] with planes normal to the paper through the dashed lines in (a). [The delay times τ at the four Reynolds numbers are 162, 144, 144, and 108 ms, respectively; about 40 of the 300 orbits observed at each Reynolds number are shown in (a).]

been developed for circle maps.

Unfortunately, the existent circle-map theory does not apply to the quasiperiodic to chaotic transition in the Couette-Taylor system, because frequency locking is not observed. In fact, Rand has shown that frequency locking *cannot* occur in systems with circular symmetry.[20] Thus the breakup of the 2-torus in systems such as the Couette-Taylor system, rotating concentric spheres, and the differentially heated rotating annulus must occur in a way that is different from the systems described by maps with a cubic inflection point.

Considering again the circle maps in Fig. 7, we should point out that although the loss of invertibility of the circle map appears to occur approximately at the Reynolds number corresponding to the onset of chaos, it is difficult to determine precisely the Reynolds number at which the map becomes noninvertible. This difficulty arises because the appearance of the map depends to some degree on the choice of the delay time and the location of the Poincaré section and on the origin of the polar coordinate system. With the delay time chosen to be far from the value corresponding to the first minimum in the mutual information or with the coordinate system origin purposely located far off center, we found that we could obtain noninvertible maps in the quasiperiodic flow regime, below the onset of chaos. Therefore, we can only say that the association of the loss of invertibility of the circle map with the onset of chaos is suggestive rather than conclusive in our experiments. It is certainly clear, however, that further theoretical and experimental study of circle maps in systems with rotational symmetry is warranted.

IV. ATTRACTOR DIMENSION

As we have shown, the photographs, power spectra, and phase portraits indicate that the nonperiodic Couette-Taylor flow is deterministic. We will now show that the strange attractor is low dimensional, and in doing this we will examine several effects that could influence the result of dimension calculations.[5]

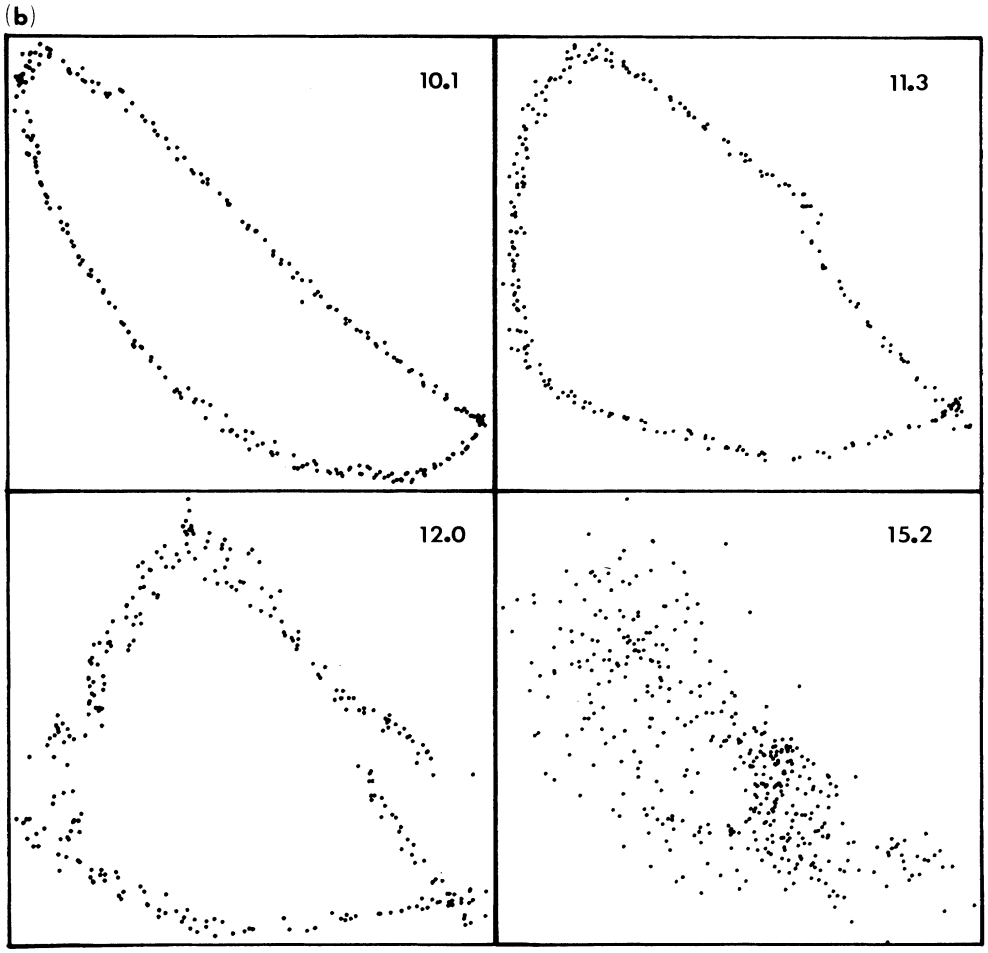

FIG. 6. (*Continued*).

We have computed the pointwise dimension d_μ (Farmer *et al.*[1]) and the correlation dimension ν (Grassberger and Procaccia[36]), both of which are based on the idea that the number of points $N(\epsilon)$ in a ball of radius ϵ scales with the dimension d, $N(\epsilon) \propto \epsilon^d$. The pointwise and correlation dimensions are given by

$$d_\mu = \lim_{\epsilon \to 0} \frac{\langle \ln N(\epsilon) \rangle_x}{\ln \epsilon} , \tag{1}$$

$$\nu = \lim_{\epsilon \to 0} \frac{\ln \langle N(\epsilon) \rangle_x}{\ln \epsilon} , \tag{2}$$

where the ball of radius ϵ is centered at the reference points x on the attractor, and the embedding dimension m satisfies $m \geq 2d_\mu + 1$. The quantities d_μ and ν are related by the inequality $\nu \leq d_\mu$; they can be obtained from the same algorithm simply by interchanging the logarithm and the average over different reference points x.

We find that the dimension values determined from the Couette-Taylor data satisfy the inequality $\nu \leq d_\mu$, but the difference between ν and d_μ is within the uncertainty in our dimension values; therefore, we will refer to the calculated dimension values simply as d.

For an m-dimensional embedding we usually use 2^{m+2} reference points because the reference points then fill the phase space equally densely for each value of the embedding dimension. The number of data points used in calculating the dimension is discussed in Sec. IV D below.

A. Different regions of scaling

According to Eqs. (1) and (2), the dimension should be given (in the limit $\epsilon \to 0$, for sufficiently large m) by the slopes of graphs of $\log_{10} N(\epsilon)$ versus $\log_{10} \epsilon$; Fig. 8(a) shows such a graph. Graphs of the local slope, $d[\log_{10} N(\epsilon)]/d(\log_{10} \epsilon)$, such as shown in Fig. 8(b), are very helpful in understanding the ϵ dependence of $N(\epsilon)$ for laboratory data, since the limit $\epsilon \to 0$ obviously cannot be taken due to experimental noise and the finite amount of data.

Consider the four distinct regions shown in Fig. 8(b): In region A, the number of points in a ball and the slope both approach zero as ϵ approaches zero because of the finite number of data points. For slightly larger ϵ, region B, the instrumental or measurement noise is dominant—the balls are smaller than the smallest temporal and spatial scales that can be resolved in the experiment. Since random noise fills all dimensions of phase space, the slope

in this region approaches the value of embedding dimension m as ϵ is decreased. With a very large number of points the slope would attain a value equal to embedding dimension before the data-limited region, region A, would be reached. However, in the example in Fig. 8(b), the data file size limitation is reached at a slope of about 3.7, well before a slope equal to the embedding dimension ($m=6$) is attained; with further decrease in ϵ, the slope then begins to decrease. This transition from region B to region A would occur at smaller ϵ if the number of data points were increased, but there would always be a transition from region B to region A for any data file with a finite number of points.

Region C is the region of primary interest: the constant non-integer-valued slope reflects the fractal structure of the strange attractor. The value of the slope is the dimension of the attractor if the embedding dimension is sufficiently large (see next subsection).

Finally, in region D the ball size ϵ approaches the size

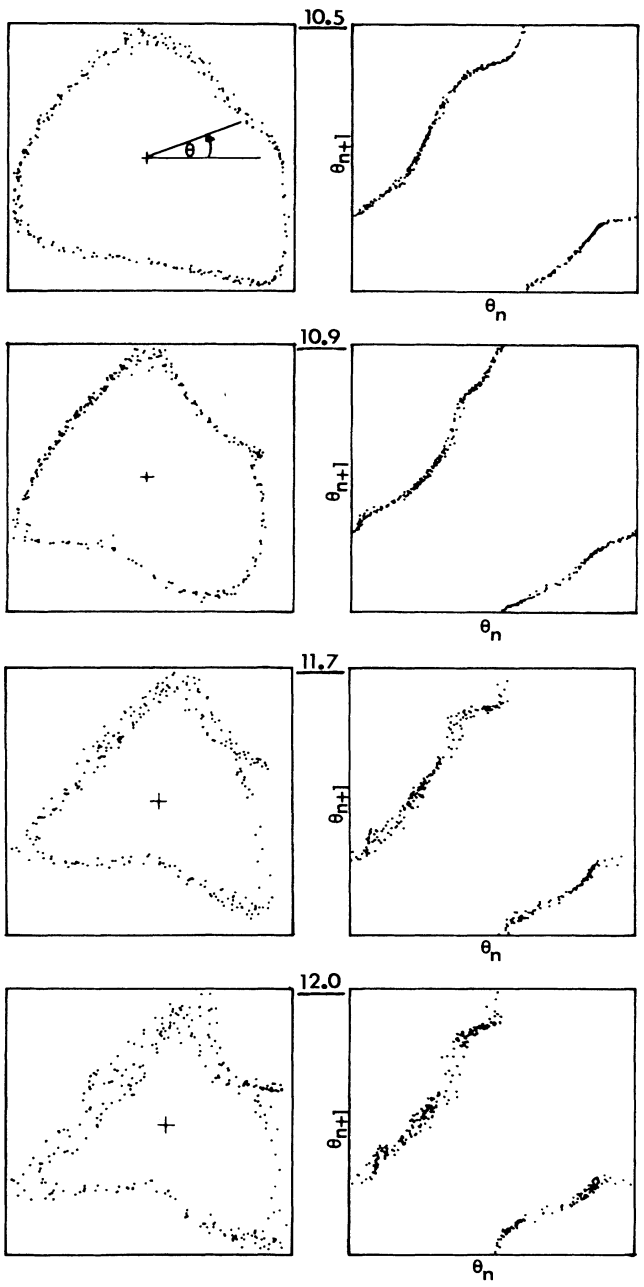

FIG. 7. The Poincaré sections shown on the left were used to construct maps of the circle shown on the right, θ_{n+1} versus θ_n, $\theta\epsilon[0,2\pi]$. The crosses in the Poincaré sections show the origins of the polar coordinate systems. At $R/R_c=10.5$ and 10.9 the maps are invertible; at $R/R_c=11.7$ the map has become fuzzy and the slope appears to be about zero for two values of θ_n; and at $R/R_c=12.0$ the map has developed a relative maximum and is no longer invertible.

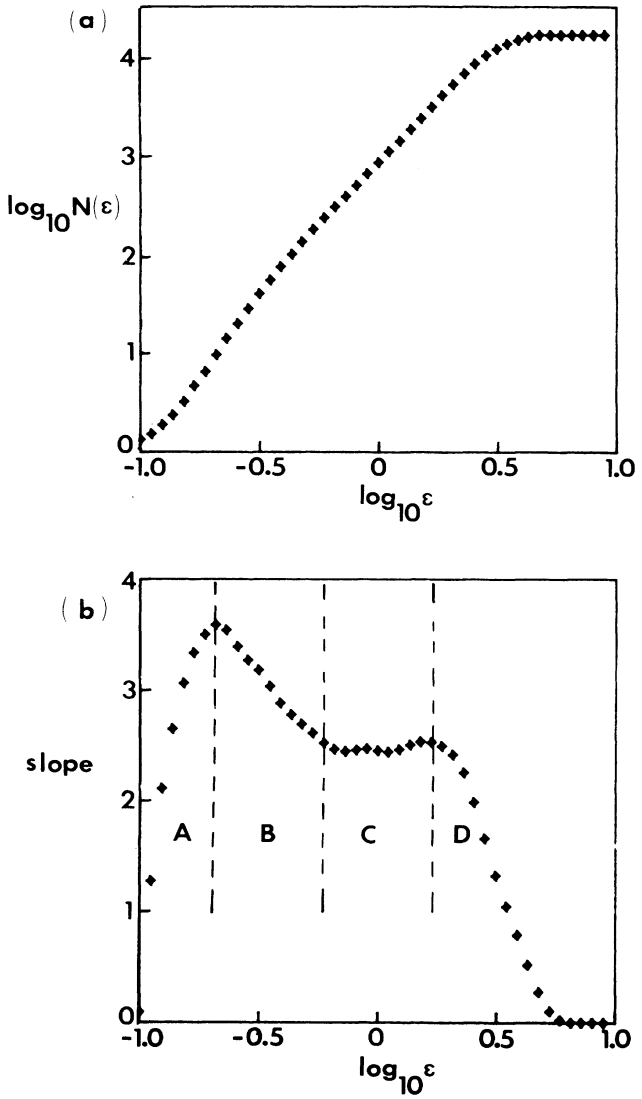

FIG. 8. (a) The number of points $N(\epsilon)$ inside a ball of radius ϵ, averaged over 256 reference points, for a strange attractor with 16384 points. (The ball radius ϵ is the velocity in cm/s.) (b) The local slope of (a), $d[\log_{10}N(\epsilon)]/d(\log_{10}\epsilon)$ as a function of the ball radius ϵ. Regions A, B, C, and D are discussed in the text. The slope in the scaling region, region C, yields $d=2.4$. ($R/R_c=12.4$; $m=6$; $\tau=182$ ms)

of the attractor, and N saturates at a value corresponding to the total number of data points; hence the slope approaches zero. Around the transition from region C to D the slope increases for some systems. The reason for this is that the ball radius approaches the edge of the attractor where the curvature of the attractor contributes a larger amount of data.

A major problem in extracting dimension values from laboratory data is that the noise level can be so large that it is difficult to distinguish regions B and C. Reliable values of d can be obtained only if region C is fairly broad. Indeed, the idea of a self-similar fractal structure of an attractor is meaningful only if it occurs for a fairly wide range in ϵ. Wide scaling regions can be achieved only with a high signal-to-noise ratio and large numbers of data points (see Sec. IV D); otherwise, region B will extend to such large ϵ that no scaling region will be discernible. In our experiments region C extends over more than an order of magnitude range in ϵ at small Reynolds numbers, but for $R/R_c > 17$ the plateau corresponding to the self-similar structure is hardly discernible. Longer data files and more precise data are needed to obtain wider scaling regions.

Another source of error arises in averaging over several reference points: different regions on the attractor can show different scaling behavior at a given length scale.[5(c)] Then averaging $N(\epsilon)$ over all reference points with ϵ fixed yields erroneous values of d. This problem is most serious when the scaling region (region C) is very narrow. In this case the scaling about individual reference points should be examined before averaging. We have done this at $R/R_c = 19.0$, where the averaged data show no well-defined scaling region, and we have found that about half of the randomly selected reference points have a scaling region. Not surprisingly, the scaling regions occur at different ϵ for different reference points. However, it is not simple to define a reliable procedure for choosing the scaling regions for individual reference points in the case of experimental data; therefore, our dimension values for $R/R_c > 17$ (see Sec IV G) have a large uncertainty.

B. Embedding dimension

The effect of varying the embedding dimension m is illustrated in Fig. 9. According to the embedding theorem,[27] the reconstructed phase space must have a dimension m of at most $2d + 1$ to ensure an embedding of the attractor. For m too small, projection effects could reduce the apparent dimensionality of an attractor. For each set of data we computed d as a function of m, and we found that usually we had to increase m to nearly $2d + 1$ before the value deduced for d became independent of m; see Fig. 9.

C. Delay time

A poor choice of delay time τ can result in a very narrow scaling region, or there can be an apparent scaling region that does not actually correspond to the dimension of the attractor, or there may even be no scaling region at all. For example, if τ is too small, the attractor can be so flat that a ball with a radius equal to the instrumental noise scale will also span the thickness of the entire attractor. The effect of varying delay times is illustrated in Fig. 10, which shows graphs of the slope $d[\log_{10}N(\epsilon)]/d(\log_{10}\epsilon)$ computed for delay times corresponding to the attractors shown in Figs. 5(b), 5(c), and 5(d). For the optimum delay time, corresponding to the first minimum in the mutual information, the width of the scaling region [see Fig. 10(b)] is larger than for shorter [Fig. 10(a)] or longer [Fig. 10(c)] delay times.

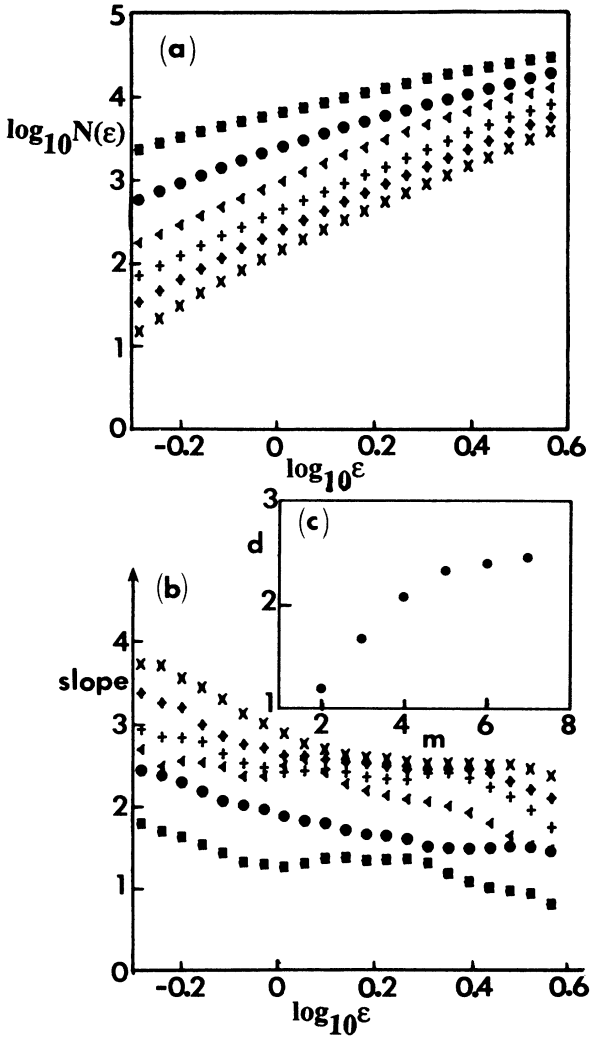

FIG. 9. The effect of varying the embedding dimension m is illustrated with data obtained at $R/R_c = 16.0$. (■, $m=2$; ●, $m=3$; ◀, $m=4$; +, $m=5$; ◆, $m=6$; and ×, $m=7$). (a) The dependence of the average number of points $N(\epsilon)$ in a ball on the radius ϵ of the ball. The data file has 32 768 points, and 2^{m+2} reference points were used in obtaining the average of $\log_{10}N(\epsilon)$. (b) The slope of the curves shown in (a) as a function of ϵ. (c) The slope of the curves in the scaling region as a function of m. The value of the dimension d is given by the asymptotic value of the slope at large m, which is 2.5.

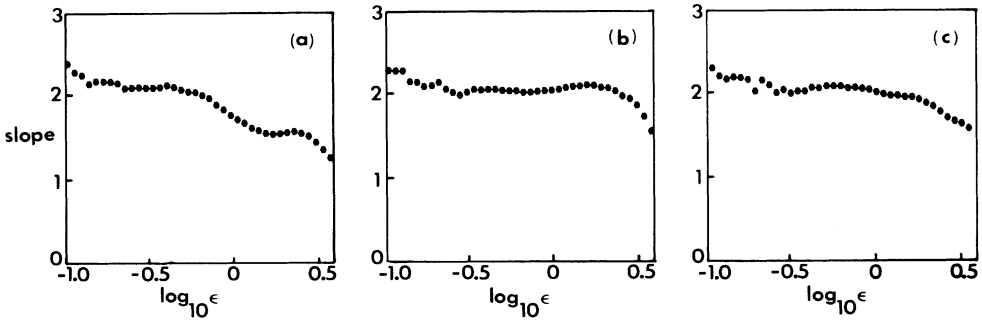

FIG. 10. The slope $d[\log_{10}N(\epsilon)]/d(\log_{10}\epsilon)$ for the data shown in Fig. 5: (a) $\tau/T_2=0.11$, which is smaller than the optimum value of τ; (b) $\tau/T_2=0.24$, which is the optimum τ; and (c) $\tau/T_2=0.48$, which is larger than the optimum τ. The scaling region where the slope is constant is wider for the optimum choice of τ.

D. Data requirements

The number of data points necessary to determine the dimension of an attractor depends on the structure of the attractor, the dimension of the attractor, and the sampling rate. To our knowledge there have been no systematic numerical or analytic studies of the data requirements for determining the dimension of strange attractors, but the number of points necessary to resolve an attractor down to a length scale ϵ increases exponentially with increasing dimension.[3] Therefore, the analysis of high-dimensional attractors by the techniques we have used will require extremely large data files. However, Sornerjai[5(e)] has recently proposed that "*calibrated*" algorithms could be used to obtain reasonable estimates of dimension from fairly small data sets. This intriguing possibility should be carefully examined in a future study.

We have found that the accuracy in the value of d deduced for a given number of points depends on the sampling rate. Broomhead and King[37] give a lower bound on the sampling time, but we know of no criterion for choosing the optimum sampling rate. We have tested the influence of sampling time for model systems such as the Rössler and Lorenz attractors,[38] and have found that the broadest scaling regions (region C in Fig. 8) are obtained for about 10—30 points per orbit; the size of the scaling region shrinks for larger or smaller sampling rates. In our experiment we have used rates of 10—100 points per orbit.

We have examined the number of data points n necessary to determine the dimension of one of our attractors for Couette-Taylor flow, and the results are shown in Fig. 11. The sampling rate was held fixed at about 35 points/orbit. It is evident that, as n is increased, the size of the scaling region extends to lower and lower ϵ. Only 400 data points provide enough resolution to resolve the attractor at large ϵ. However, n should also be large enough to resolve scales down to the noise scale, and this requires several thousand points for this 2.4-dimensional attractor, as Fig. 11 illustrates.

E. Analysis of random numbers

Guckenheimer has used the order statistics of independent random variables to examine problems attendant with obtaining accurate dimension estimates for randomly distributed points.[3(b)] Here we illustrate some of these problems by applying our dimension algorithm to randomly distributed data.

The number of points required to achieve an average separation ϵ in a d-dimensional space of linear extent L is $(L/\epsilon)^d$. Since the determination of dimension from Eq. (1) or (2) requires taking the limit $\epsilon\rightarrow 0$, the average separation should be small, say 3% or less of the linear

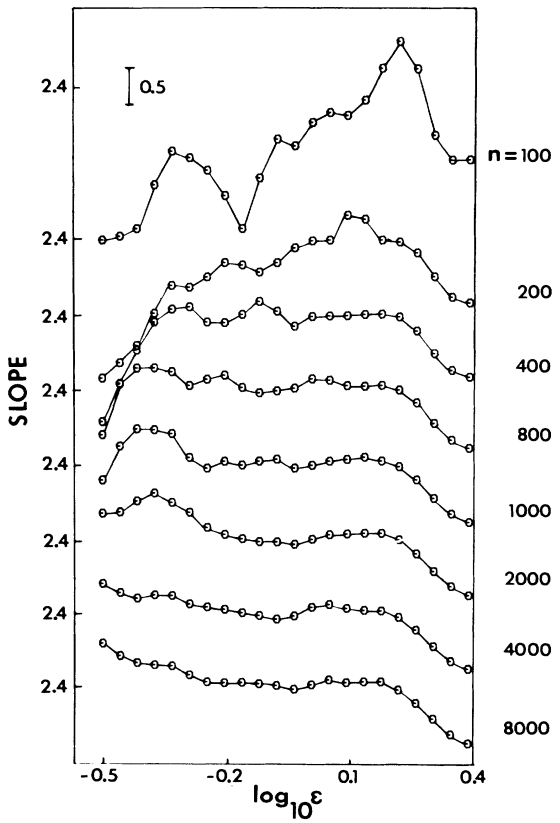

FIG. 11. The dependence of the slope $d[\log_{10}N(\epsilon)]/d(\log_{10}\epsilon)$ on the number of data points n for data obtained at $R/R_c=12.0$. A file with 32 768 points yields $d=2.4$. ($m=7$)

extent. This would require 4×10^4 points in a three-dimensional space and 5×10^{10} points in a seven-dimensional space.

We have determined numerically the approximate width of the scaling range, $\Delta\log_{10}\epsilon$, for randomly distributed points in hypercubes with dimension $m=2$, 3, and 4. Independently generated random numbers were used for each coordinate. The number of points n necessary to achieve scaling ranges $\Delta\log_{10}\epsilon$ of widths 0.4 and 0.8 was determined as a function of m, as shown in Fig. 12. Although the determination of the width of the scaling region is imprecise, the results suggest that the required number of data points increases slightly faster than 10^m. We should mention that even for the largest number of points (10^7), the value of d given by the slopes of the $\log_{10}N$ versus $\log_{10}\epsilon$ graphs was a few percent smaller than m.

In the next numerical experiment we investigated the number of points required to determine the dimension of randomly distributed points in a ten-dimensional space. The value of d obtained for 10^7 points was about 9, but d was still increasing with increasing n, as Fig. 13 illustrates. Both for the present case and for the two-, three-, and four-dimensional spaces discussed in the previous paragraph we thought that the difference between the dimension deduced from the data and the dimension of the space could perhaps arise from a deterministic property of the random-number generators. However, we tried two different 64-bit random-number generators (the Cray Fortran routine RANF and the IMSL routine GGUW) on a Cray X-MP computer, and no difference was found.

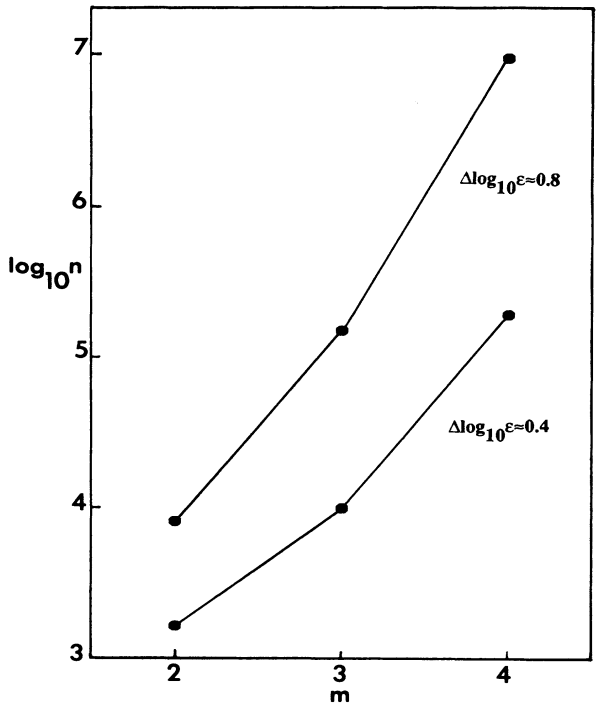

FIG. 12. The number of points n required to achieve scaling ranges (region C in Fig. 8) of width 0.4 and 0.8 for two-, three-, and four-dimensional hypercubes containing randomly distributed points. The analysis used 100 randomly chosen reference points; 1000 reference points were found to yield smoother curves in the scaling region, but the dimension estimates were not significantly improved.

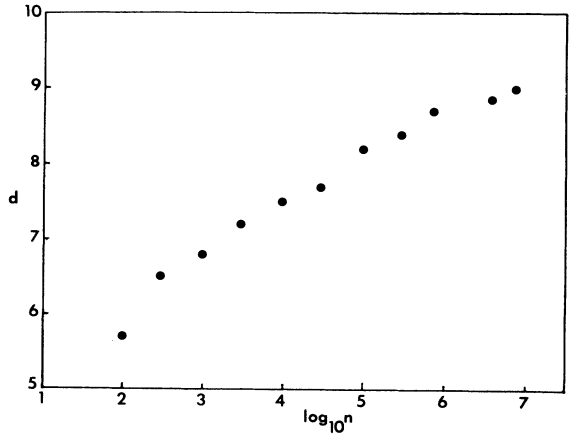

FIG. 13. The value of d determined from the dimension algorithm for a ten-dimensional hypercube containing n randomly distributed points. The analysis used 100 randomly chosen reference points.

The dimension estimates in Fig. 13 are low primarily because of edge effects [see Ref. 3(b), p. 361]. That is, the increase in the number of points within a ball of radius ϵ is slower for a ball whose center is near an edge of the space than for a ball located far from any edge.[3,10] Figure 14 shows that for 300 000 points randomly distributed in a ten-dimensional space, the value of d increases from 8.4 when the location of the reference points is unrestricted, to $d=9.2$ when the reference points are required to be at least 12% (of the linear extent) from an edge.

These considerations of dimension calculations for randomly distributed points provide at best only a qualitative guide to the importance of different effects for strange at-

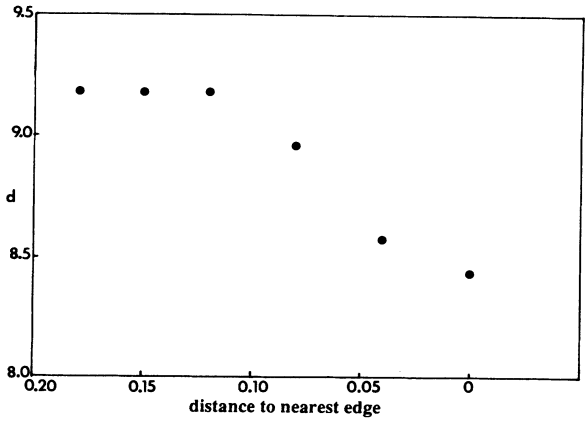

FIG. 14. The dependence of d on the location of the reference points for 300 000 randomly distributed points in a ten-dimensional hypercube. The abscissa gives the maximum distance from the reference points to the edge of the box, expressed as a fraction of the size of the box; the 100 reference points were randomly located inside this smaller box.

tractors, which of course have highly complicated structures. The effect of the location of the reference points will vary for different deterministic systems. For example, a 2-torus has no edge, while for other systems the influence of edges increases with the dimension of the attractor.

F. Filtering effect

Experimental data are often low-pass filtered, either in the process of acquiring the data or later by software. Low-pass filtering can not only influence the noise scale, but also, if the filtering is very severe, it can reduce the number of degrees of freedom that can be detected. The effect on Couette-Taylor data obtained at $R/R_c = 12.0$ is shown in Fig. 15, where reducing the filter cutoff from $20\omega/\Omega$ to $5\omega/\Omega$ reduces the value determined for d. In our experiment we did not apply any filter other than those given by the acquisition process.

G. Dimension of the Couette-Taylor attractor

Figure 16 shows the dimension of the Couette-Taylor attractor as a function of the Reynolds number. The uncertainty in d, which arises from the various effects we have discussed, increases from 0.1 for $d \approx 2$, to 0.4 for $d \approx 3$ ($R/R_c \approx 17$). The error increases rapidly with further increase in Reynolds number because, as discussed in Sec. IV A, it becomes difficult to discern a scaling region; the dimension values shown for $R/R_c > 17$ are included only to indicate the continuing increase in the dimension with increasing Reynolds number.

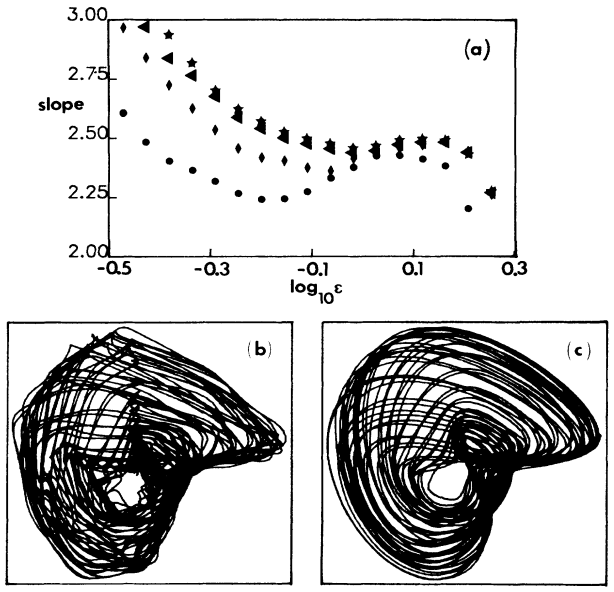

FIG. 15. The effect of low pass filtering of Couette-Taylor data obtained at $R/R_c = 12.0$. (a) The slopes of $\log_{10}N(\epsilon)$ vs $\log_{10}\epsilon$ graphs are shown for four cutoff frequencies: ●, $5/\Omega$; ◆, $10/\Omega$; ◀, $15/\Omega$; and ★, $20/\Omega$. (b) Phase portrait for a cut-off frequency of $20/\Omega$. (c) Phase portrait for a cut-off frequency of $5/\Omega$.

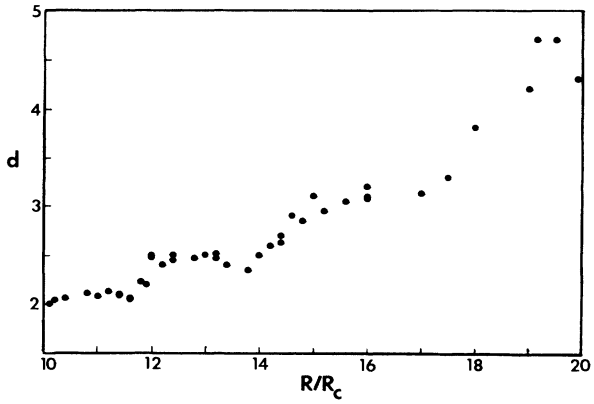

FIG. 16. The dimension of the Couette-Taylor attractor as a function of the Reynolds number.

The results for the dimension show that the onset of chaotic flow occurs at $R/R_c = 11.7 \pm 0.2$.[19] When the Reynolds number is increased beyond the onset of chaos, the value of the dimension increases monotonically except for small dips at $R/R_c = 11.7$ and 13.7. These dips are possibly a consequence of the fact that at these Reynolds numbers the ratio of the two fundamental frequencies happens to be near simple rational numbers; therefore, the torus is not covered well by the data—longer data files may be needed at these Reynolds numbers.

The reproducibility of the values determined for the dimension was quite good. Measurements were made over a period of six months, during which time the cylinder system was disassembled and reassembled several times, and the dimension values were found to reproduce to a much better precision than that indicated by the quoted uncertainties.

V. DISCUSSION

We have shown that the dimension of the attractors in the Couette-Taylor experiment is 2.0 for modulated wavy vortex flow. When the Reynolds number is increased beyond $R/R_c = 11.7 \pm 0.2$, the dimension becomes noninteger, increasing above the value 2.0. At this same Reynolds number broadband noise appears in the power spectrum and the largest Lyapunov exponent becomes positive, thus providing further evidence that $R/R_c = 11.7 \pm 0.2$ marks the onset of chaos.[19] The exponential decay of the power spectrum provides additional evidence that the observed nonperiodic behavior corresponds to low-dimensional deterministic chaos, not stochastic behavior.

The dimension values should be viewed as characterizing the flow in the *entire* annulus: measurements that were made at different spatial points for the same Reynolds number yielded (within the quoted uncertainties) the same value for the dimension. The dimension values seem remarkably small when one examines the photographs of the flow, particularly at the larger Reynolds numbers, say $R/R_c = 17$ (see Fig. 1). The dimension calculation suggests that, even for this noisy looking flow, only a small number of degrees of freedom may be relevant to the

dynamics.

We have emphasized some of the pitfalls in the determination of dimension. It is not difficult to develop an algorithm that will yield numbers that can be called dimension, but it is far more difficult to be confident that those numbers truly represent the dynamics of the system under study. We have examined briefly some of the requirements for data to be used in determining dimension and have found that the number of data points needed increases dramatically with increasing d, at least for the techniques for computing dimension [Eqs. (1) and (2)] that we have used. There is clearly a great need for systematic numerical and analytic studies of the potential and the limitations of dimension calculations.

Another problem that warrants further study is the question of the route to chaos in systems with rotational symmetry. The well-studied routes to chaos—period doubling, intermittency (tangent bifurcations), and the breakup of a 2-torus as described by circle maps—apparently do not occur in this system.[39] As we have shown, circle maps can be obtained from the data for the Couette-Taylor system, but the behavior of these maps is apparently quite different from the maps that exhibit frequency locking. Thus there is a need for numerical and analytic studies of models with rotational symmetry and for further experiments on the transition to chaos for different conditions in rotationally symmetric systems.

ACKNOWLEDGMENTS

This work was supported in part by National Science Foundation (NSF) Grant No. MSM-82-06889 and in part by the U.S. Office of Naval Research and U.S. National Aeronautics and Space Administration (NASA) through the NASA-Ames Research Center, Moffet Field, California under Interchange No. NCA2-1R781-401.

[1]J. D. Farmer, E. Ott, and J. A. Yorke, Physica **7D**, 153 (1983).

[2]P. Grassberger and I. Procaccia, Phys. Rev. Lett. **50**, 346 (1983).

[3](a) J. Guckenheimer, Annu. Rev. Fluid Mech. **18**, 15 (1986); (b)Contemp. Math. **28**, 357 (1984).

[4]J. P. Eckmann and D. Ruelle, Rev. Mod. Phys. **57**, 617 (1986).

[5]Several papers in *Dimensions and Entropies in Chaotic Systems,* edited by G. Mayer-Kress (Springer, Berlin, 1986), treat problems in determining dimensions from time-series data: (a) R. Badii and A. Politi, *ibid.* p. 67; (b) F. Hunt and F. Sullivan, *ibid.* p. 74; (c) F. Holzfuss and G. Mayer-Kress, *ibid.* p. 114; (d) W. E. Caswell and J. A. Yorke, *ibid.* p. 123; (e) R. L. Somerjai, *ibid.* p. 137; (f) J. G. Caputo, B. Malraison, and P. Atten, *ibid.* p. 180.

[6]C. C. Foias, O. P. Manley, and R. Teman, J. Fluid Mech. **150**, 427 (1985).

[7]O. P. Manley and Y. M. Treve, Phys. Lett. **82A**, 88 (1981).

[8]J.-M. Ghidaglia (unpublished).

[9]A. Brandstater, J. Swift, H. L. Swinney, A. Wolf, J. D. Farmer, E. Jen, and J. P. Crutchfield, Phys. Rev. Lett. **51**, 1442 (1983); A. Brandstater, J. Swift, H. L. Swinney, and A. Wolf, in *Turbulence and Chaotic Phenomena in Fluids,* edited by T. Tatsumi (Elsevier North-Holland, Amsterdam, 1984), p. 179; A. Brandstater and H. L. Swinney, in *Fluctuations and Sensitivity in Nonequilibrium Systems,* edited by W. Horsthemke and D. Kondepudi (Springer, Berlin, 1984), p. 166; A. Brandstater, Ph.D. dissertation Universität Kiel, 1984.

[10]B. Malraison, P. Atten, P. Berge, and M. Dubois, J. Phys. (Paris) Lett. **44**, L987 (1983); P. Atten, J. G. Caputo, B. Malraison, and Y. Gagne, J. Mec. Theor. Appl., special issue (1984), p. 133; see also Ref. 5(f).

[11]J. Guckenheimer and G. Buzyna, Phys. Rev. Lett. **51**, 1438 (1983). The transition to chaos in a related system, a two-layer baroclinic fluid, has been studied by J. E. Hart, Physica **20D**, 350 (1986).

[12]R. C. DiPrima and H. L. Swinney, in *Hydrodynamic Instabilities and the Transition to Turbulence,* edited by H. L. Swinney and J. P. Gollub (Springer, Berlin, 1985), p. 139.

[13]P. Matisse and M. Gorman, Phys. Fluids **27**, 759 (1984).

[14]R. G. W. Brown, in *Photon Correlation Techniques,* edited by E. O. Schulz-DuBois (Springer, Berlin, 1982), p. 66.

[15]R. G. W. Brown and R. Jones, Opt. Lett. **8**, 449 (1983).

[16]P. R. Fenstermacher, H. L. Swinney, and J. P. Gollub, J. Fluid Mech. **94**, 103 (1979).

[17]R. S. Shaw, C. D. Andereck, L. A. Reith, and H. L. Swinney, Phys. Rev. Lett. **48**, 1172 (1981).

[18]M. Gorman and H. L. Swinney, J. Fluid Mech. **117**, 123 (1982).

[19]The uncertainty of ± 0.2 in the value of R/R_c at onset is estimated from an analysis of the photographs of the flow, velocity power spectra, phase portraits, and circle maps, and from the values deduced for the dimension and Lyapunov exponents of the attractors.

[20]D. Rand, Arch. Rat. Mech. Anal. **79**, 1 (1982); see also M. Gorman, D. Rand, and H. L. Swinney, Phys. Rev. Lett. **46**, 992 (1981).

[21]The component called ω_2 here was called ω_3 in Ref. 16.

[22]H. S. Greenside, G. Ahlers, P. C. Hohenberg, and R. W. Walden, Physica **5D**, 322 (1982).

[23]D. Sigeti and W. Horsthemke, Phys. Rev. A. **35**, xxxx (1987).

[24]G. Ahlers and R. P. Behringer, Phys. Rev. Lett. **40**, 712 (1978); G. Ahlers and R. W. Walden, *ibid.* **44**, 445 (1980).

[25]P. Atten, J. C. Lacroix, and B. Malraison, Phys. Lett. **79A**, 255 (1980).

[26]N. H. Packard, J. P. Crutchfleld, J. D. Farmer, and R. S. Shaw, Phys. Rev. Lett. **45**, 712 (1980); J. C. Roux, R. H. Simoyi, and H. L. Swinney, Physica **8D**, 257 (1983).

[27]F. Takens, in *Dynamical Systems and Turbulence,* Vol. 898 of *Lecture Notes in Mathematics,* edited by D. A. Rand and L. S. Young (Springer, Beriin, 1981), p. 366.

[28]A. M. Fraser and H. L. Swinney, Phys. Rev. A **33**, 1134 (1986).

[29]A. M. Fraser, in *Dimensions and Entropies in Chaotic Systems,* edited by G. Mayer-Kress (Springer, Berlin, 1986), p. 82; IEEE Trans. Inf. Theory (to be published).

[30]A. Wolf, J. B. Swift, H. L. Swinney, and J. A. Vastano, Physica **16D**, 285 (1985).

[31]P. Coullet, C. Tresser, and A. Arneodo, Phys. Lett. **77A**, 327 (1980).

[32]M. J. Feigenbaum, L. P. Kadanoff, and S. J. Shenker, Physica

5D, 370 (1983).
[33]S. Ostlund, D. Rand, J. Sethna, and E. Siggia, Physica **8D**, 303 (1983).
[34]M. H. Jensen, P. Bak, and T. Bohr, Phys. Rev. A **30**, 1960 (1984); T. Bohr, M. H. Jensen, and P. Bak, *ibid.* **30**, 1970 (1984).
[35]P. Cvitanovic, M. H. Jensen, L. P. Kadanoff, and I. Procaccia, Phys. Rev. Lett. **55**, 343 (1985).
[36]P. Grassberger and I. Procaccia, Physica **9D**, 189 (1983).
[37]D. S. Broomhead and G. P. King, Physica **20D**, 217 (1986).
[38]These systems are defined and discussed in Ref. 30.
[39]However, G. Pfister observed period doubling when the rotational symmetry of his Couette-Taylor system was broken by tilting one end very slightly, Proceedings of the Second International Symposium on Applications of Laser Anemometry in Fluid Mechanics, Lisbon, 1984, p. 3.2. Also, see G. Pfister, in *Flow of Real Fluids,* Vol. 235 of *Lecture Notes in Physics,* edited by E. E. A. Meier and F. Obermeier (Springer, Berlin, 1985), p. 199.

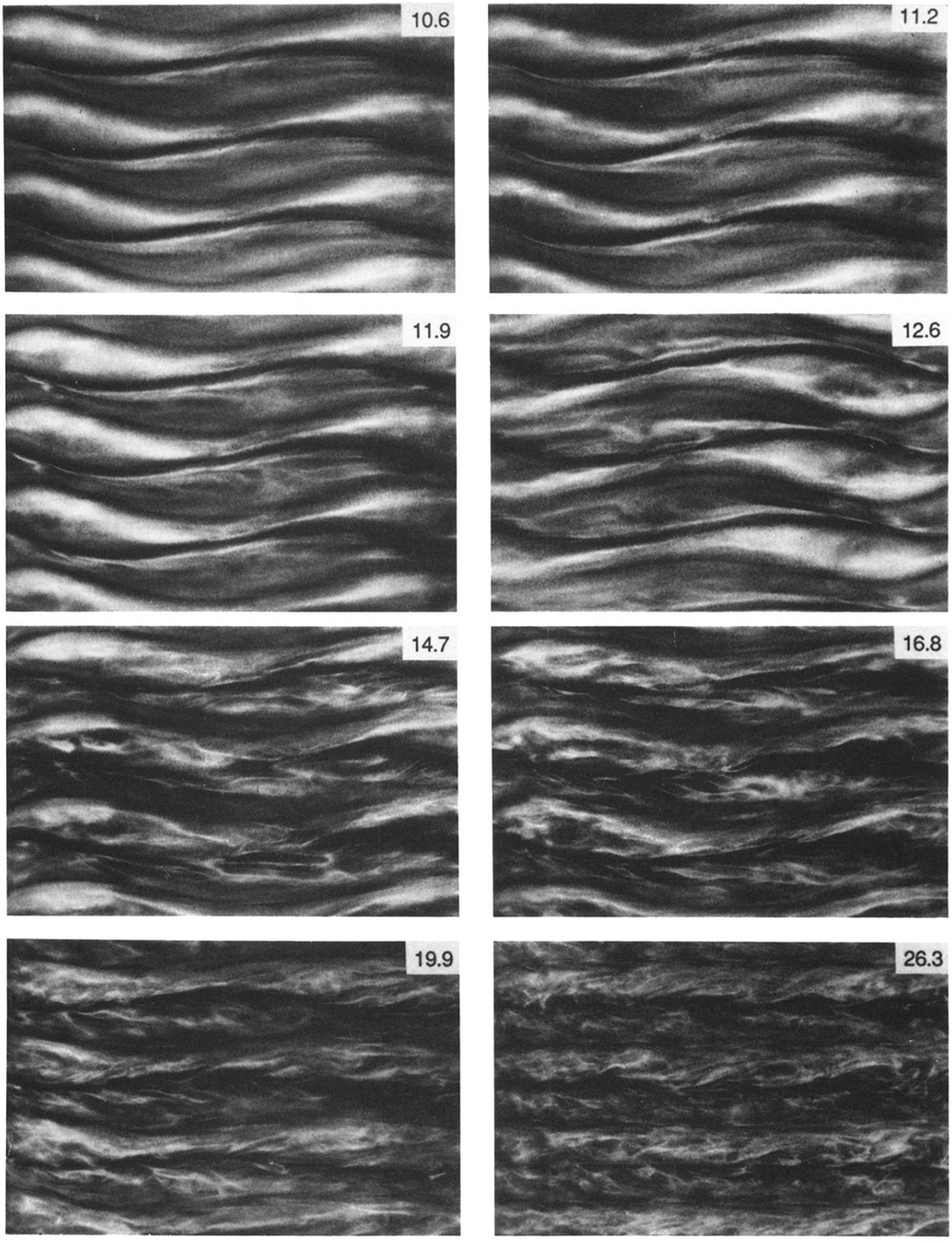

FIG. 1. Photographs of the flow as a function of Reynolds number in the region of transition from modulated wavy vortex flow to chaotic flow. The values of R/R_c are given on the photographs. The first two pictures are of modulated wavy vortex flow, while the remainder are in the chaotic regime. The flow patterns were rendered visible using a suspension of small platelets (Ref. 13).